Manipulating acoustic wave reflection by a nonlinear elastic metasurface

Xinxin Guo,[1,a)] Vitalyi E. Gusev,[1] Katia Bertoldi,[2] and Vincent Tournat[1,b)]
[1]*LAUM, CNRS UMR 6613, Le Mans Université, Av. O. Messiaen, 72085 Le Mans, France*
[2]*John A. Paulson School of Engineering and Applied Sciences, Harvard University, Cambridge, Massachusetts 02138, USA*

(Received 15 November 2017; accepted 26 February 2018; published online 27 March 2018)

The acoustic wave reflection properties of a nonlinear elastic metasurface, derived from resonant nonlinear elastic elements, are theoretically and numerically studied. The metasurface is composed of a two degree-of-freedom mass-spring system with quadratic elastic nonlinearity. The possibility of converting, during the reflection process, most of the fundamental incoming wave energy into the second harmonic wave is shown, both theoretically and numerically, by means of a proper design of the nonlinear metasurface. The theoretical results from the harmonic balance method for a monochromatic source are compared with time domain simulations for a wave packet source. This protocol allows analyzing the dynamics of the nonlinear reflection process in the metasurface as well as exploring the limits of the operating frequency bandwidth. The reported methodology can be applied to a wide variety of nonlinear metasurfaces, thus possibly extending the family of exotic nonlinear reflection processes. https://doi.org/10.1063/1.5015952

I. INTRODUCTION

The ability of locally resonant architected materials to achieve wave control at wavelengths much longer than the dimensions of the resonant elements has been demonstrated and utilized extensively over the past several years.[1–6] Slow sound,[7–9] negative refraction,[10–15] sub-wavelength wave guiding, and multiplexing,[16,17] are all among the recently reported effects of significant interest. This sub-wavelength range of operations is especially pertinent for layers made of locally resonant elements,[18,19] denoted as metasurfaces. As such, the average thickness can be drastically reduced, which is advantageous, e.g., for sound absorption,[20–27] carpet cloaking,[28–30] or other purposes. The key challenges ahead in improving and applying the proposed wave control designs, based on metamaterials, are mainly as follows: (i) the operating bandwidth, which is often limited to the resonance frequency range, (ii) the tunability of the metamaterial response, and (iii) the nonlinear (amplitude-dependent) response, as found to be particularly relevant for intense sound waves. Recent research has primarily sought to overcome the first two of these listed challenges,[31–33] whereas this paper focuses on the third challenge, i.e., the nonlinear amplitude-dependent response of metamaterials.

Compared to the linear dispersive properties of acoustic metamaterials, the nonlinear wave interaction processes in metamaterials have been studied less extensively. Nevertheless, granular crystals and granular metamaterials are structures whose contact interaction nonlinearity may be efficiently mobilized to produce nonlinear wave processes, such as asymmetric transmission,[16,34–37] nonlinear pulse and soliton propagation,[38–40] harmonic generation,[41,42] breathers,[43,44] etc. While these granular structures are among the most widely studied nonlinear elastic engineered materials for waves and despite their rich behavior, the nonlinear parameter space of granular systems is highly constrained by the intrinsic Hertz-Mindlin contact nonlinearity. Moreover, the metasurfaces configuration, in the form of a sub-wavelength layer, does not *a priori* favor the accumulation of nonlinear effects along distances, as classically observed in homogeneous media.[45,46] Recent results on architected soft solids[40,47–51] however have demonstrated some ways of managing the dynamic elastic nonlinearity and offered other ways of designing nonlinear resonating elements for elastic and acoustic wave control in propagation or in metasurface configurations.

This article sets out to show that unusual reflection effects by a nonlinear metasurface can indeed be modeled and predicted. More specifically, it demonstrates the ability to avoid reflection at the fundamental incident frequency and to convert most of the energy in the reflection process into the second harmonic wave. The metasurface configurations explored are found to be realistic for subsequent implementation in experimental testing. The theoretical analysis methodology developed can be applied to other nonlinear metasurface designs and other nonlinear effects. The first part of this paper studies the case of a reflected monochromatic incident stress wave, while the second part numerically analyzes the nonlinear reflection of a wave packet, in addition to studying the frequency bandwidth character (or time-domain effects) of the nonlinear reflection process.

II. THE PROBLEM UNDER CONSIDERATION AND THE CORRESPONDING METASURFACE DESIGN

We consider herein the problem of wave reflection by a sub-wavelength thickness metasurface, in a one-dimensional

Note: This paper is part of the Special Topic section "Acoustic Metamaterials and Metasurfaces" published in Journal of Applied Physics Volume **123**, Issue 9, 07 March 2018.

[a)]Electronic mail: xinxin.guo.etu@univ-lemans.fr
[b)]Electronic mail: vincent.tournat@univ-lemans.fr

configuration, i.e., with normal incidence on the flat surface. The incoming wave is a longitudinal scalar wave, such as an acoustic wave in a fluid or a pure longitudinal stress wave in a homogeneous solid. The propagation medium is assumed to be semi-infinite. The unit cell of the metasurface is composed of two elementary masses (m_1 and m_2) connected to two nonlinear springs (K_1^{NL} and K_2^{NL}) and viscous dampers (Γ), as shown in Fig. 1. The metasurface thickness is assumed to be much less than the wavelength in the propagation medium (1). Springs and dampers are regularly positioned over the metasurface, with each occupying a lateral surface S.

A quadratic nonlinearity is considered for both springs: this nonlinearity follows a force-displacement law expressed as $F_i = K_i(\Delta\ell_i) + \beta_i K_i(\Delta\ell_i)^2$ (i = 1, 2) with $\Delta\ell_i$ being the elongation of spring i and β_i the quadratic nonlinear parameter.

The metasurface is inserted between a semi-infinite propagation medium (1) and a rigid wall (2). Let us consider a plane stress-wave σ_{inc} of amplitude σ_0 incoming from $-\infty$ and propagating along the positive x direction. The problem is therefore one-dimensional, and the incident and reflected waves can be written as a function of $x - ct$ and of $x + ct$, respectively (using the time convention $i\omega t$), with c the wave velocity in the propagation medium. The total stress σ can be decomposed into an incoming stress-wave and a reflected stress-wave $\sigma = \sigma_{inc} + \sigma_{ref}$; the following can now be written: $\frac{\partial\sigma}{\partial x} = -\frac{1}{c}\frac{\partial\sigma_{inc}}{\partial t} + \frac{1}{c}\frac{\partial\sigma_{ref}}{\partial t}$. The one-dimensional wave equation, $\rho\frac{\partial^2 u_x}{\partial t^2} = -\frac{\partial\sigma}{\partial x}$, with ρ the mass density of the propagation medium, must be satisfied on the metasurface at $x = 0$, which leads to the following useful relation: $\sigma_{ref} = \sigma_{inc} + \rho c\frac{\partial u_1}{\partial t}$.

The system of metasurface motion equations can thus be written in the following form:

$$\begin{cases} m_1\dfrac{\partial^2 u_1}{\partial t^2} = -\left(2\sigma_{inc} + \rho c\dfrac{\partial u_1}{\partial t}\right)S - K_1(u_1 - u_2) - \Gamma\dfrac{\partial(u_1 - u_2)}{\partial t} - \beta_1 K_1(u_1 - u_2)^2, \\ m_2\dfrac{\partial^2 u_2}{\partial t^2} = K_1(u_1 - u_2) + \Gamma\dfrac{\partial(u_1 - u_2)}{\partial t} + \beta_1 K_1(u_1 - u_2)^2 - K_2 u_2 - \Gamma\dfrac{\partial u_2}{\partial t} - \beta_2 K_2 u_2^2, \end{cases} \tag{1}$$

with S being the characteristic lateral surface area of each metasurface element and u_i (i = 1, 2) the displacement of mass m_i.

The analysis is carried out here for metasurface parameters defined using ratios between the two masses, i.e., $m_2/m_1 = 2$, and the two linear spring constants, i.e., $K_2/K_1 = 2$, while the dashpots are characterized by a damping coefficient Γ identical for both. Consequently, the proposed interface design, in the linear case, leads to a dual-resonance system characterized by the following relation between the two angular resonance frequencies $\omega_2 = 2\omega_1$

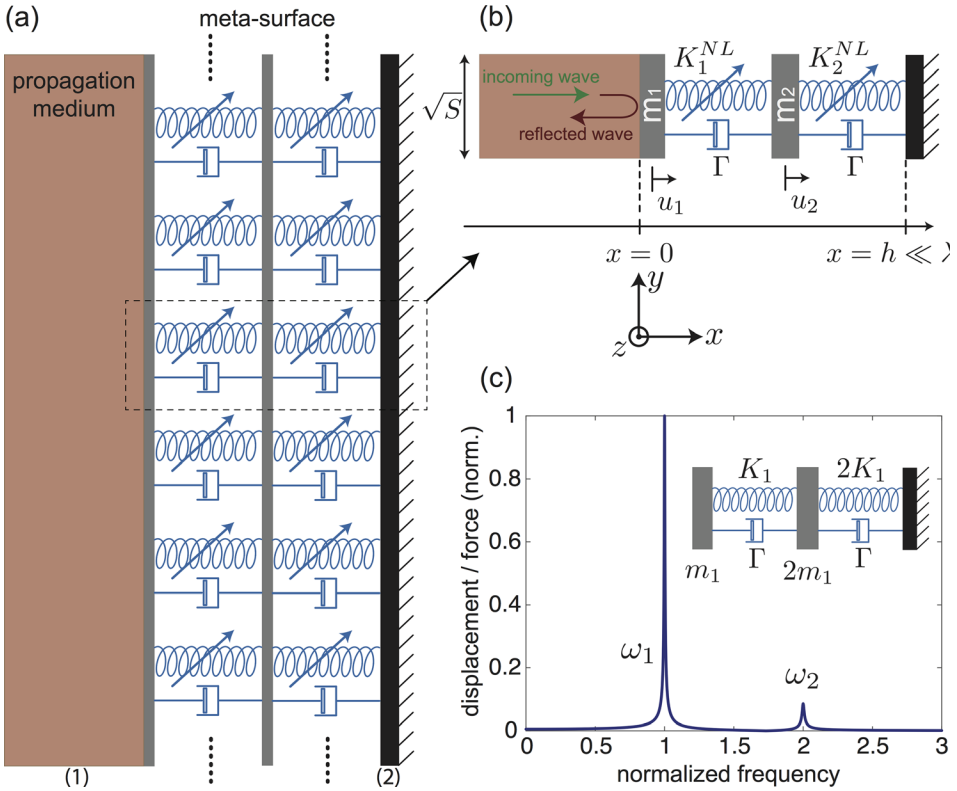

FIG. 1. Design of the nonlinear elastic metasurface by (a) a vertically periodic structure at the sub-wavelength scale; in order to simplify the analysis, (b) a dual-resonance model with two mass-spring elements is implemented. A semi-infinite medium (1) and a rigid wall (2) are separated by the designed metasurface. It is assumed herein that all model elements of the model are capable of only moving along the x-direction, while the nonlinearities are only presented in the two springs; (c) presents the frequency response in the linear case of the first mass, with the proposed model featuring two resonance frequencies, i.e., ω_1 and ω_2.

$= 2\sqrt{K_1/2m_1}$. An example of such a metasurface response function in the case without coupling in the presence of a propagation medium (vacuum) is shown in Fig. 1(c). In using the first resonance frequency ω_1, let us define the dimensionless impedance parameter γ representing the ratio of the impedance of the propagation medium to the mechanical impedance of the metasurface as follows:

$$\gamma = \frac{\rho c S}{2m_1\omega_1}. \tag{2}$$

The metasurface absorption parameter is defined as

$$\eta = \frac{\Gamma}{2m_1\omega_1}. \tag{3}$$

Using this expression, let us now define the quality factor $Q = 1/\sqrt{2}\eta$ which quantifies the effect of viscous damping in the metasurface based on the expression for a single damped mass-spring system. Moreover, let us define the dimensionless nonlinear parameters (or amplitude parameters of our problem): $B_i = \beta_i u_0$, with $u_0 = \sigma_0 S/K_1$. The motion equation system (1) can then be rewritten with dimensionless parameters as follows:

$$\begin{cases} \frac{1}{2}\Omega^2\frac{\partial^2 U_1}{\partial\tau^2} = -2f(\tau) - \gamma\Omega\frac{\partial U_1}{\partial\tau} - (U_1 - U_2) - \eta\Omega\frac{\partial(U_1 - U_2)}{\partial\tau} - B_1(U_1 - U_2)^2, \\ \Omega^2\frac{\partial^2 U_2}{\partial\tau^2} = (U_1 - U_2) + \eta\Omega\frac{\partial(U_1 - U_2)}{\partial\tau} + B_1(U_1 - U_2)^2 - 2U_2 - \eta\Omega\frac{\partial U_2}{\partial\tau} - 2B_2U_2^2, \end{cases} \tag{4}$$

where $\tau = \omega t$ is the dimensionless time, $\Omega = \omega/\omega_1$ is the normalized excitation frequency, $f(\tau) = \sigma_{inc}(\tau)/\sigma_0$ is the normalized incident stress wave at the interface $x = 0$, and $U_i = u_i/u_0$ (i = 1, 2) is the normalized displacement of each mass m_i.

In the weakly nonlinear regime of the metasurface operation, let us assume that the reflected wave spectrum from a monochromatic incident wave will contain, at the first order, combination frequencies of ω, i.e., harmonics of the incident wave. Consequently, at the boundary $x = 0$, the complex amplitude of the reflected stress wave is written as $\tilde{\sigma}_R = \tilde{\sigma_0}\sum_{n=1}^{N}\tilde{R}_n(n\Omega)e^{in\Omega\tau}$, with $\tilde{\sigma}_0$ being the complex amplitude of the incident wave. Here, $\tilde{R}_n(n\Omega)$ $(1 \le n \le N)$ actually corresponds to the complex amplitudes of each reflected harmonic relative to the incident wave amplitude. In the following, for the sake of simplicity, $\tilde{R}_n(n\Omega)$ will denote the complex reflection coefficient of the n-th harmonic.

III. THEORETICAL RESULTS AND PARAMETRIC ANALYSIS: CASE OF A MONOCHROMATIC SOURCE

In the case of a monochromatic source, i.e., $f(\tau) = \cos(\tau)$, the considered motion equation system in Eq. (4) can be solved by using the Harmonic Balance Method (HBM)[52] (see the Appendix). According to this method, the solution U_i is developed in the form of a sum of all harmonics generated

$$U_i(\tau) = U_{i0} + \sum_{n=1}^{N}[C_{in}\cos(n\tau) + S_{in}\sin(n\tau)], \tag{5}$$

where U_{i0} indicates the constant terms, C_{in} and S_{in} the magnitudes of the sinusoidal terms cos and sin, respectively, and N the finite number of harmonics being considered. In the present study, which deals with weak quadratic nonlinearity, we verified that $N = 10$ is always sufficient since it yields results with relative error of less than 10^{-15} as compared to $N = 9$. By means of this explicit expression of the solution, the system in Eq. (4) is simplified and capable of being solved numerically by applying the classical Newton-Raphson method. The complex reflection coefficients of each harmonic component n are then deduced as follows:

$$\tilde{R}_n = \delta_{n1} + i\gamma n\Omega(C_{1n} - iS_{1n}), \tag{6}$$

where δ_{n1} is the Delta function, which is always zero except when $n = 1$. The results obtained are considered to be the theoretical. Section IV will compare these results to the case of a wave packet source in order to study the effects of finite bandwidth.

In the present study, the excitation frequency ω is always set equal to the first resonance frequency ω_1 of the linearized metasurface, i.e., the normalized excitation frequency is $\Omega = 1$. According to the theoretical results produced by the HBM method (Fig. 2), in order to obtain an optimal generation of the second or third harmonic component, the nonlinear parameters B_i need to be carefully chosen. When the two springs of the model have the same nonlinearity ($B_1 = B_2$), higher harmonics are not necessarily generated during the reflection process, see, for example, the value of $|\tilde{R}_2|$ along the diagonal $B_1 = B_2$ in Fig. 2(b). To enhance the nonlinear process of second harmonic generation, the difference between nonlinear parameters B_1 and B_2 must be as large as possible. In the following study therefore, we have set $B_2 = 0$; moreover, the maximum value of B_1 is defined such that the ratio of the nonlinear part of the elastic force to its linear part is approximately 0.1, which means that the nonlinearity remains weak. For the illustrated case in Fig. 2 with an impedance parameter $\gamma = 0.0162$ and an absorption parameter $\eta = 0.0088$, the defined maximum value of B_1 equals roughly 0.002.

Furthermore, for the proposed linear properties of the metasurface, the second resonance lies at a frequency corresponding to twice that of the first resonance, i.e., $\omega_2 = 2\omega_1$. Consequently, when the system is excited at the first

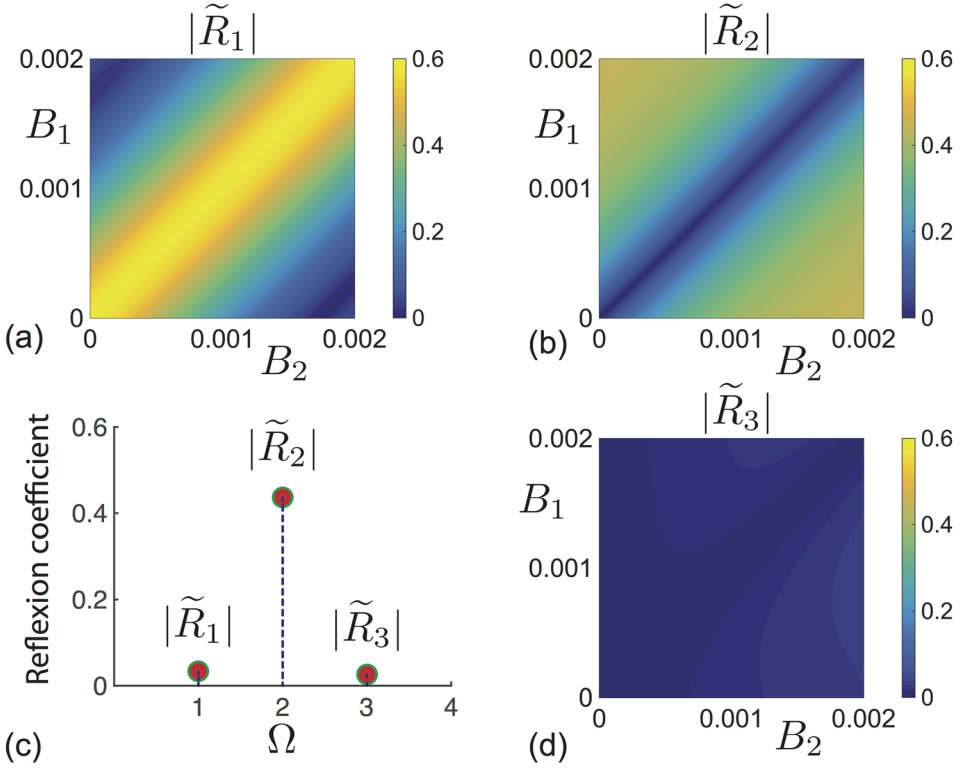

FIG. 2. Theoretical magnitudes of the reflection coefficients for (a) the reflected fundamental wave, (b) the reflected second harmonic, and (d) the reflected third harmonic, derived by HBM, as a function of the nonlinear parameter values B_1 and B_2. (c) shows an example of a special case with $B_1 = 0.0018$ and $B_2 = 0.0002$. The graphs have been produced with an impedance parameter $\gamma = 0.0162$ and an absorption parameter $\eta = 0.0088$.

resonance frequency $\omega = \omega_1$, the second harmonic, which is generated at 2ω (and thus effectively "reflected") due to the quadratic nonlinearity, coincides with the second resonance frequency of the metasurface. Thanks to this selected resonance frequency matching and with appropriate nonlinear parameters [e.g., $B_2 \ll B_1 < 0.02$ see Fig. 2(c)], the reflected second harmonic can thus be well amplified. Simultaneously, we have found that the other higher harmonics are nearly all missing, and even more interestingly, the fundamental wave has almost been entirely eliminated during the reflection, i.e., $|\tilde{R}_1| \ll 1$.

Let us now examine the role of the impedance parameter γ and the absorption parameter η on this nonlinear process of reflection, which converts a large amount of the energy from the incoming fundamental wave into the second harmonic reflected wave. By studying the linear case ($B_i = 0$ with $i = 1, 2$) for the designed interface, it is possible to determine the characteristic times of each resonance: at the first resonance frequency ω_1, the dimensionless characteristic times of absorption (losses due to the dashpots) and impedance (losses due to radiation in the propagation medium) are $\tau_1^{abs} = \frac{3}{\eta}$ and $\tau_1^{imp} = \frac{3}{2\gamma}$, respectively, At the second resonance frequency ω_2, they become $\tau_2^{abs} = \frac{3}{5\eta}$ and $\tau_2^{imp} = \frac{3}{\gamma}$. These characteristic times lead to the definition of the dimensionless lifetime τ_i ($i = 1, 2$) for each resonance

$$\frac{1}{\tau_i} = \frac{1}{\tau_i^{abs}} + \frac{1}{\tau_i^{imp}}. \tag{7}$$

In the linear case, the reflection coefficient of the fundamental wave can be obtained analytically in the following form:

$$\tilde{R}_1 = \frac{(1/2)(\Omega^2-1)(\Omega^2-4) + i\eta\Omega(-2\Omega^2+3) - i\gamma\Omega(-\Omega^2+3) - \eta(\eta-2\gamma)\Omega^2}{(1/2)(\Omega^2-1)(\Omega^2-4) + i\eta\Omega(-2\Omega^2+3) + i\gamma\Omega(-\Omega^2+3) - \eta(\eta+2\gamma)\Omega^2}. \tag{8}$$

Hence, without nonlinearity, when the excitation occurs at the first resonance frequency ($\Omega = 1$), the reflection can be eliminated if the characteristic impedance time is equal to the characteristic absorption time $\tau_1^{imp} = \tau_1^{abs}$, i.e., equivalent to $\eta = 2\gamma$. This condition is highlighted in Fig. 3(a) with a dashed line, and the corresponding computed values of $|\tilde{R}_1|$ are observed to be very low. For the studied quadratic nonlinear case (with $B_1 \neq 0$ and $B_2 = 0$, the dimensionless characteristic time of nonlinearity has also been defined as $\tau^{NL} = 1/\sqrt{B_1}$, which conveys an analogous physical meaning to the shock formation characteristic distance for a nonlinear propagating wave:[46] the nonlinear effects can efficiently develop for characteristic times of metasurface vibration longer than τ^{NL}. One consequence of this approach is that $\tau_{NL} < \tau_i$ ($i = 1, 2$) is required for a nonlinear effect to efficiently develop, i.e., before the resonance vanishes. This condition for the significant nonlinear effect development can be verified with the results from Figs. 3(a) and 3(b). In the cross-hatched region of Fig. 3(a), where $\tau_{NL} < \tau_1$, $|\tilde{R}_1|$ is no longer zero along the dashed line $\tau_1^{imp} = \tau_1^{abs}$, thus

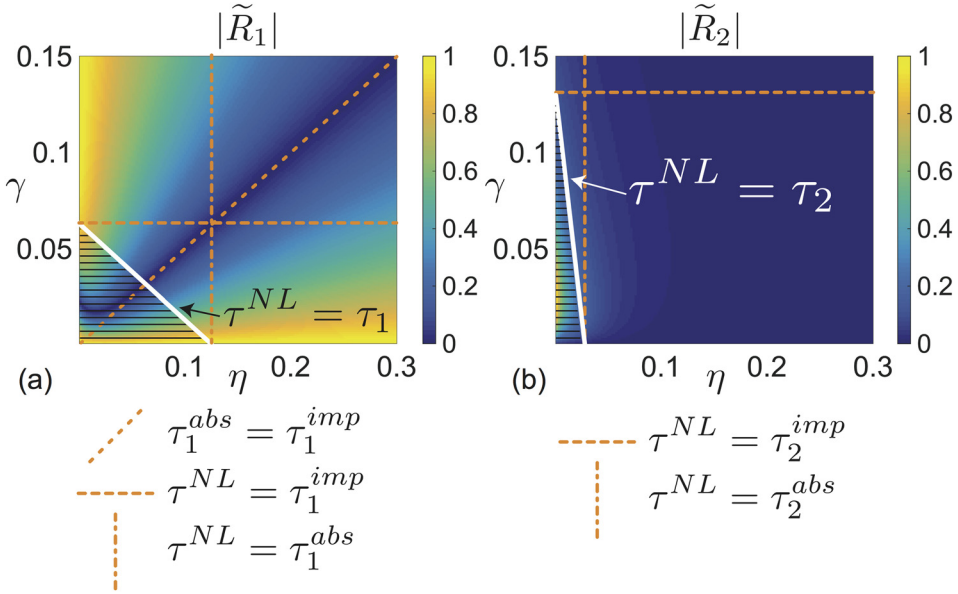

FIG. 3. Magnitude of the theoretical reflection coefficient (a) at the incoming fundamental frequency and (b) for the reflected second harmonic wave. $|\tilde{R}_1|$ and $|\tilde{R}_2|$ are obtained via the HBM with a monochromatic source and are evaluated as a function of both the impedance parameter γ and the absorption parameter η. The nonlinear parameters are fixed at $B_1 = 0.002$ and $B_2 = 0$. The dashed lines show the characteristic parameter equalities. The cross-hatched regions in both (a) and (b) highlight the parameter space characterized by $\tau^{NL} < \tau_{1,2}$ where nonlinear effects develop efficiently.

deviating from the linear case. In Fig. 3(b), the greatest magnitudes for $|\tilde{R}_2|$ occur in the lower left part of the graph, in the cross-hatched region where the inequality $\tau_{NL} < \tau_2$ is satisfied.

More precisely, when B_1 is set at $B_1 = 0.002$, $\tau^{NL} = \tau_1^{abs}$ (respectively, $\tau^{NL} = \tau_1^{imp}$) when $\eta \approx 0.134$ (respectively, $\gamma \approx 0.067$), and $\tau^{NL} = \tau_2^{abs}$ (respectively, $\tau^{NL} = \tau_2^{imp}$) for $\eta \approx 0.027$ (respectively, $\gamma \approx 0.134$). Hence, in order to satisfy the condition $\tau_{NL} < \tau_i$ $(i = 1,\ 2)$, $\gamma = \frac{\rho c S}{2m_1\omega_1}$ and $\eta = \frac{\Gamma}{2m_1\omega_1}$ should be much less than 1. Physically, this condition means that the propagation medium should actually be much softer than the metasurface. It also means that the metasurface should be weakly dissipative, i.e., the quality factor Q should not be too low, and typically much greater than unity.

In the results presented in Fig. 2, the value $\gamma = 0.0162$ has been chosen. Considering air as the propagation medium, this value of γ leads to a resonance frequency $f_r = 2$ kHz for a metasurface with a mass per unit area equal to one, which can be achieved with a solid like balsa wood (density of $130\,\mathrm{kg/m^3}$), and a thickness of 7.7 mm. Similarly, the choice $\eta = 0.0088$ used for Fig. 2 corresponds to a quality factor $Q = 80$. This configuration example, based on such realistic parameter values, shows the potential for applying the presented concept to the nonlinear manipulation of airborne sound. Note that in the linear case (i.e., $B_1 = B_2 = 0$), the assigned values of parameters γ and η lead to a fundamental reflection coefficient $|\tilde{R}_1| \approx 0.57$. However, when the nonlinear parameter B_1 is nonzero and limited such that the ratio of the nonlinear part of the elastic force to its linear part is at most 0.1, e.g., $B_1 = 0.002$, the fundamental reflection can nearly vanish (with $|\tilde{R}_1| \approx 0.07$), while the second harmonic can be efficiently generated and reflected with a reflection coefficient greater than 0.45. As such, the ratio between $|\tilde{R}_2|$ and $|\tilde{R}_1|$ exceeds 6. Therefore, even with very limited nonlinearity (e.g., a nonlinear elastic force ten times smaller than the linear elastic force), a nearly full conversion from the fundamental incoming energy to the second harmonic reflection can be achieved by the proposed metasurface design. The conversion result presented herein can be further improved if the impedance parameter is changed to $\gamma = 0.0176$, thus providing a fundamental reflection coefficient of $|\tilde{R}_1| \approx 0.005$ and a second harmonic reflection coefficient of $|\tilde{R}_2| \approx 0.46$.

This theoretical study based on the HBM demonstrates a valuable energy transfer, from a fundamental wave to its second harmonic in the reflection process by means of a nonlinear metasurface. The preconditions for efficient conversion are now in place and provide the design rules for metasurface element characterization. These results remain valid for a monochromatic incident wave. Section IV will focus on analyzing the case of a finite-length wave packet in order to extend the operating conditions of such a nonlinear metasurface and verifying the robustness of the highlighted effects.

IV. NUMERICAL RESULTS AND PARAMETRIC ANALYSIS WITH A WAVE PACKET SOURCE

The following discussion will consider a Gaussian modulated wave packet of the form:

$$\sigma_{inc}(\tau)/\sigma_0 = f(\tau) = \sin(\tau) e^{-\frac{(\tau-\tau_0)^2}{(\omega T)^2}},$$

as the incident wave, with $\tau = \omega t$, T the characteristic temporal width of the wave packet, and τ_0 the dimensionless time center of the packet. A classical fourth-order Runge-Kutta integration method (RK4)[53] is used to solve the system of temporal equations, in Eq. (1), for all cases presented in this section. Other numerical integration methods have been implemented to verify these RK4 results, i.e., 6th order Runge-Kutta, Matlab functions ODE45 and ODE133, and Adams methods. By introducing the relation $\sigma_{ref} = \sigma_{inc} + \rho c \frac{\partial u_1}{\partial t}$, the reflected wave signal is obtained once the temporal displacements u_i have been determined. The time-frequency analysis of the reflected signals can then be performed using the spectrogram method, yielding, in particular, a reflected time- and frequency-dependent magnitude $|\tilde{R}|$.

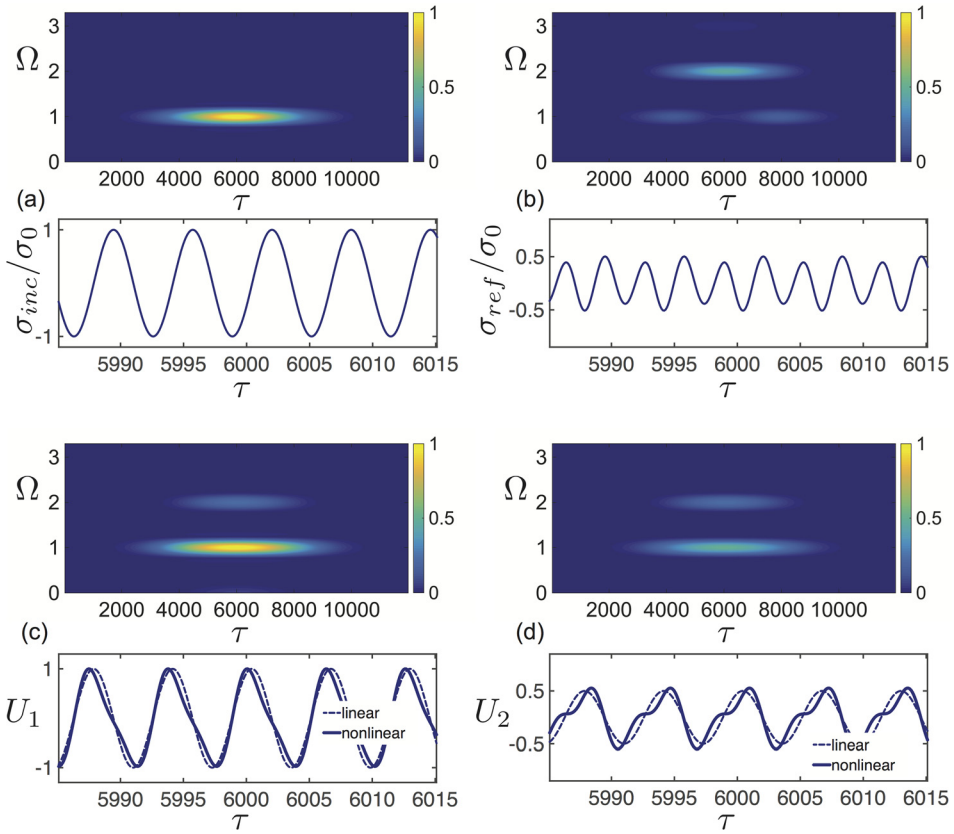

FIG. 4. Spectrogram and waveform of (a) normalized incident wave σ_{inc}/σ_0, of (b) reflected wave normalized by incident amplitude σ_{ref}/σ_0, and of (c) and (d) displacements of the two masses, respectively, u_1 and u_2, normalized by the maximum displacement of the first mass $max(U_1)$. These results have been obtained numerically by means of the fourth-order Runge-Kutta method (RK4) with a wave packet source of dimensionless width $\omega T = 2000$. The illustrated waveforms have been extracted around the time center t_0 of the source ($\tau = \omega t_0 = 6000$). System parameters are fixed at $\gamma = 0.0162$, $\eta = 0.0088$ (corresponding to $Q = 80$), $B_1 = 0.002$ and $B_2 = 0$.

When the metasurface is excited by a wave packet with a carrier frequency equal to the first resonance frequency of the metasurface ($\omega = \omega_1$), the two masses of the metasurface start vibrating with the same phase and at an amplitude ratio of 2 (corresponding to the eigenmode $\{u_1, u_2\}_1^T = \{2, 1\}^T$ of the first resonance). During the increase in metasurface vibration amplitude, i.e., as the displacement magnitudes of both masses are rising, higher harmonics are gradually being generated, to an increasing extent, and the mass displacement waveforms are being distorted (see Fig. 4). More specifically, as observed in Sec. III, among all the higher harmonics generated, energy is mainly converted to the second harmonic component due to frequency matching with the second metasurface resonance, i.e., $2\omega = \omega_2$. At 2ω, the displacement relationship between the two masses follows the eigenmode $\{u_1, u_2\}_2^T = \{-1, 1\}^T$ of the second metasurface resonance, i.e., the same displacement magnitude for both masses yet with out-of-phase motion. In Fig. 4, the spectrograms and zooms of the waveforms of both the incident and reflected stress waves are plotted, along with the displacements of the two masses.

If the incident wave packet lasts long enough, the theoretical results derived via the HBM in Sec. III should be replicated. This outcome can be verified by monitoring the maximum of $|\tilde{R}(\Omega)|$ and of $|\tilde{R}(2\Omega)|$ from the spectrogram contained in Fig. 4 for various temporal widths T of the incident wave packet. A good level of agreement has been obtained between the theoretical HBM results and the temporal simulation for a wave packet when the dimensionless characteristic width ωT of the wave packet is much larger than the characteristic lifetime of the metasurface resonances, i.e., $\omega T \gg \tau_i$ with $i = 1, 2$. With the chosen values of impedance parameter $\gamma = 0.0162$ and absorption parameter $\eta = 0.0088$, the lifetimes of the first and second resonances are $\tau_1 \approx 72.82$ and $\tau_2 \approx 49.83$. With $B_1 = 0.002$, the characteristic time of nonlinearity $\tau^{NL} = 1/\sqrt{B_1} \approx 22.36$, which satisfies the condition $\tau^{NL} < \tau_i$ for high nonlinear effect efficiency. In turn the inequality $\omega T \gg \tau^{NL}$ with $i = 1, 2$ needs to be satisfied in order to retrieve the HBM results for continuous excitation with a wave packet of temporal width T.

In Fig. 4(b), it is observed that the steady state regime is reached at $\tau = 6000$, where the amplitude of the fundamental reflected wave is at a minimum and the amplitude of the reflected second harmonic wave is at a maximum. The local values of $|\tilde{R}_2| \sim 0.5$ and $|\tilde{R}_1| \sim 0$ closely correspond to the HBM results values [see Fig. 2(c)]. To study the robustness of this effect for various signal characteristic widths ωT, we performed a number of numerical simulations for $15 \leq \omega T \leq 566$, i.e., equivalent to $4 \leq N_T \leq 150$, where N_T is the number of fundamental carrier wave periods within the packet width at half its maximum amplitude. For an N_T typically less than 10, however, the frequency width of each contribution (whether fundamental or second harmonic) cannot be easily separated in the time frequency analysis. Consequently, we opted to monitor the values at $\Omega = 1$ and at $\Omega = 2$ of the Fourier spectrum for the entire reflected wave signals. These results are displayed in Fig. 5 for the reflection at the fundamental frequency $|\tilde{R}(\Omega = 1)| = |\tilde{R}_1|$ and in Fig. 6 for the reflection at the second harmonic frequency $|\tilde{R}(\Omega = 2)| = |\tilde{R}_2|$, for various metasurface parameters.

In Fig. 5(a), the reflection coefficient magnitude at the fundamental frequency $|\tilde{R}_1|$ is plotted for various values of

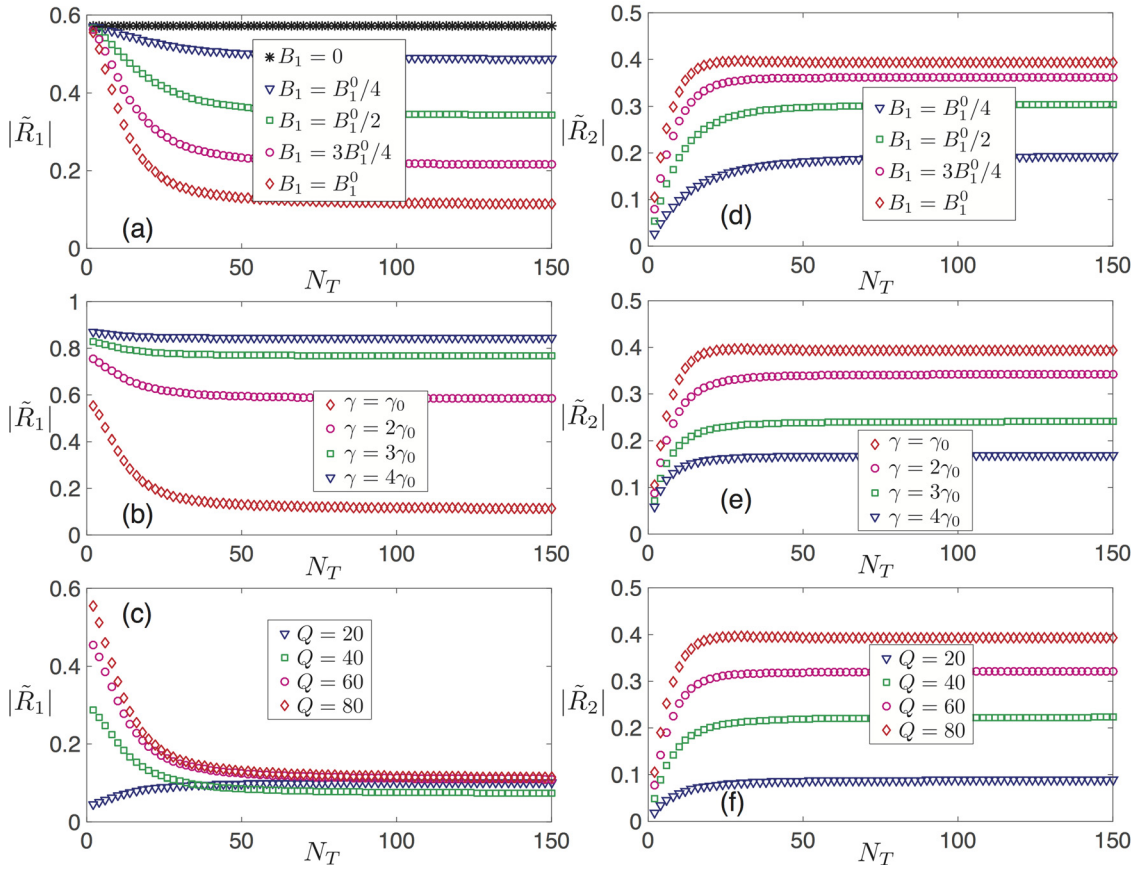

FIG. 5. Magnitude of the reflection coefficient at the fundamental frequency (three left-hand figures) and the second harmonic frequency (three right-hand figures) obtained from the Fourier spectrum for the entire reflected wave taken at $\Omega = 2$, with various wave packet source widths (N_T denotes the number of carrier wave periods within the width at half height of the wave packet source). In all graphs, the default parameters are impedance parameter $\gamma_0 = 0.0162$, quality factor $Q = 80$ ($\Longleftrightarrow \eta_0 = 0.0088$), and nonlinear parameters $B_1 = B_1^0 = 0.002$, $B_2 = 0$. Otherwise, all parameter values are indicated in the graph legend.

the nonlinear parameter B_1 from 0 to $B_1 = B_1^0 = 0.002$. For this metasurface configuration, the linear case ($B_1 = B_2 = 0$) shows that $|\tilde{R}_1|$ is close to 0.6 for any wave packet source width. With nonlinearity (i.e., $B_1 \neq 0$), $|\tilde{R}_1|$ decreases as wave packet width N_T increases, thus revealing the existence of a nonlinear effect that depends on N_T (and obviously on B_1). For $B_1 = B_1^0 = 0.002$, $|\tilde{R}_1|$ decreases as N_T rises to ~25 and then stabilizes, reaching the asymptotical value of ~0.1. This value is greater than what had been obtained for the same metasurface parameters with the HBM because the Fourier spectrum over the entire reflected signal necessarily comprises transient effects, e.g., the increasing front of the wave packet amplitude, where nonlinear effects cannot fully develop due to insufficient amplitude. On all the curves in Fig. 5, the reflection coefficients are nearly constant for a wave packet width $N_T > N_T^c \simeq 25$.

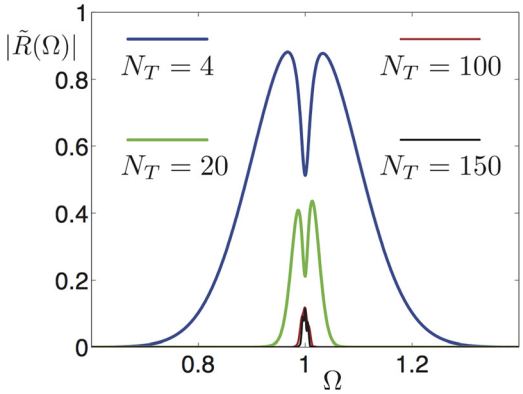

FIG. 6. The Fast Fourier Transform (FFT) of normalized reflected wave σ_{ref}/σ_0 present around the fundamental harmonic ω for various source widths, with N_T denoting the number of periods at half height of the incident stress wave and using parameters of the system are fixed as above: $\gamma = 0.0162$, $\eta = 0.0088$ (corresponding to a Q factor equal to 80), $B_1 = 0.002$ and $B_2 = 0$.

In Fig. 5(b), for adequately long source signals ($N_T > 50$), the asymptotic values of $|\tilde{R}_1|$ depend on γ. For $\gamma = \gamma_0$ and $N_T > N_T^c$, $|\tilde{R}_1| \simeq 0.1$, while for $\gamma = 2\gamma_0$ and $N_T > N_T^c$, $|\tilde{R}_1| \simeq 0.6$. Also, as γ increases, the influence of N_T on $|\tilde{R}_1|$ tends to vanish. We found this behavior to be caused by the fact that increasing γ moves further from the efficient nonlinear effect region of the metasurface parameters, as denoted by the cross-hatched zone in Fig. 3 and defined by $\tau^{NL} < \tau_i$. Increasing γ corresponds to leaving this cross-hatched region vertically upward. As a consequence, the nonlinear effects on $|\tilde{R}_1|$ vanish and we find once again a near constant $|\tilde{R}_1|$ as a function of N_T, i.e., similar to the linear case $B_1 = 0$ exhibited in Fig. 5(a).

The influence of the resonance quality factor on $|\tilde{R}_1|$ is shown in Fig. 5(c). For large N_T values, the influence of Q is noticeable yet weak. In this case, the nonlinear effects fully

develop, and the parameter η (or Q) no longer plays an important role anymore [cross-hatched region $\tau^{NL} < \tau_1$ in Fig. 3(a) where the blue zone of small $|\tilde{R}_1|$ extends almost horizontally]. For small N_T values, however, the metasurface configurations basically reveal different behaviors: as N_T decreases, $|\tilde{R}_1|$ drops for $Q = 20$ while rises for $Q = 40$, 60, and 80. In the linear case, the configuration with $Q = 20$ actually corresponds almost perfectly to the total absorption case (or zero reflection case) $\eta = 2\gamma$, and $|\tilde{R}_1| \approx 0$ is expected. As discussed above, as N_T decreases, the nonlinear effects cannot fully develop and the results converge on the linear effects [see Fig. 5(a)]. For $Q = 20$, the linear case corresponds to a nearly perfect absorption by the metasurface, and this perfect absorption becomes degraded by the nonlinear effects occurring at higher value of N_T. Such is not the case for the other configurations with different Q values, where the nonlinear effects tend to decrease $|\tilde{R}_1|$ and improve the absorption at $\Omega = 1$ through the energy transfer to $\Omega = 2$ as N_T increases.

The reflection coefficient magnitude at the second harmonic frequency is analyzed for the same metasurface configurations as that of the fundamental frequency. In all cases, the reflection coefficient magnitude $|\tilde{R}_2|$ starts at a value close to zero for small N_T values and increases to reach a plateau after $N_T \sim 25$. The values attained for large N_T depend on the configuration and among the presented set of metasurface parameters, the largest $|\tilde{R}_2|$ is obtained for the default parameters $\gamma_0 = 0.0162$, $Q = 80$, and $B_1^0 = 0.002$.

In the aim of illustrating the spectral and temporal characteristics of the wave packet reflection process, the total signal spectra have been plotted in Fig. 6 for frequencies $\sim\Omega$ and in Fig. 7 for frequencies $\sim 2\Omega$. Four characteristic wave packet widths are considered, namely, $N_T = 4$, 20, 100, and 150. In Fig. 6, the energy absorption and nonlinear energy transfer by the nonlinear metasurface toward the harmonics in the reflection process are displayed by a dip at $\Omega = 1$ in the initial Gaussian spectrum. The nonlinear energy transfer toward the second harmonic is observed in Fig. 7 with the spectra displayed for $\Omega \sim 2$, i.e., over a frequency range in which no energy is present in the incident wave packet. The temporal signals associated with these spectra are shown in Figs. 8 and 9, respectively. It can be observed that for the

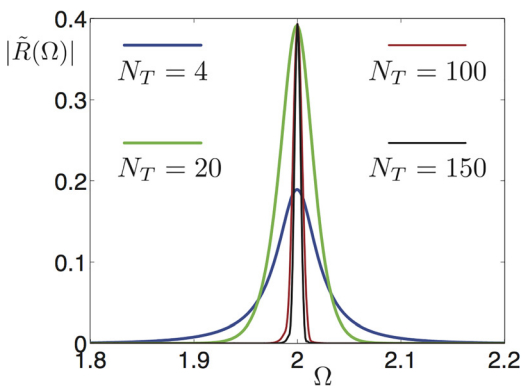

FIG. 7. The FFT of normalized reflected wave σ_{ref}/σ_0 present around the second harmonic 2ω for various source widths, with N_T denoting the number of periods at half height of the incident stress wave and using parameters of the system are fixed as above: $\gamma = 0.0162$, $\eta = 0.0088$ (corresponding to a Q factor equal to 80), $B_1 = 0.002$ and $B_2 = 0$.

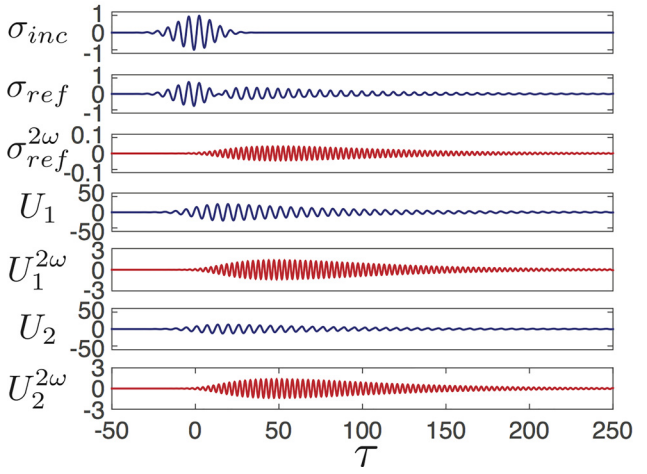

FIG. 8. Temporal signals of the wave packet source σ_{inc} with the number of periods at half height equal to $N_T = 4$, of the corresponding normalized reflected wave σ_{ref}/σ_0, and of the normalized displacements of two masses U_1 and U_2 [with normalization $U_i = u_i/u_0, (i = 1, 2)$]. The second harmonic component (in red lines) for the reflected wave and for the displacements $\sigma_{ref}^{2\omega}$ and $U_i^{2\omega}$ is obtained by applying around 2ω (from 1.5ω to 2.5ω) a bandpass filter to each original temporal signals, respectively. Using the parameters of the system, the following are fixed as above: $\gamma = 0.0162$, $\eta = 0.0088$ (corresponding to Q factor equal to 80), $B_1 = 0.002$ and $B_2 = 0$.

default set of metasurface parameters delays occur when establishing the resonances in displacements U_1 and U_2 relative to the incident wave packet, as would be expected for the transient excitation of a resonant system. Consequently, the local minimum in the reflected wave amplitude is also delayed with the respect to the central time of the incident stress wave packet. Lastly, the maximum of the temporal wave packet filtered at the second harmonic frequency is even more heavily delayed, thus demonstrating the additional time required for the nonlinear energy transfer (or nonlinear accumulation time τ^{NL}) in the metasurface.

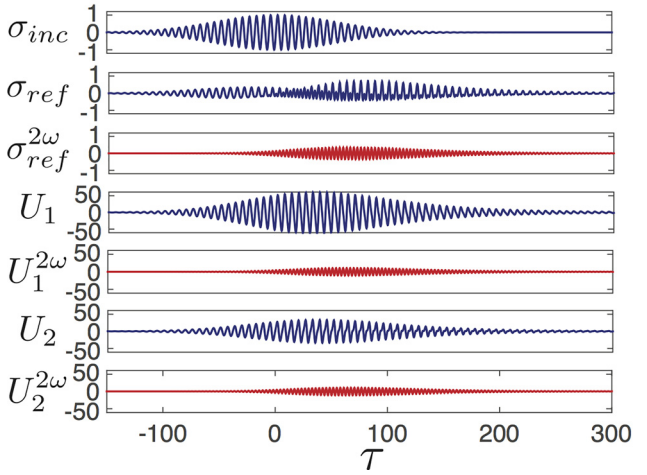

FIG. 9. Temporal signals of the wave packet source σ_{inc} along with the number of periods at the half height equal to $N_T = 20$, of the corresponding normalized reflected wave σ_{ref}/σ_0, and of the normalized displacements of two masses U_1 and U_2 [with normalization $U_i = u_i/u_0, (i = 1, 2)$]. The second harmonic component (shown in red lines) for both the reflected wave and for the displacements $\sigma_{ref}^{2\omega}$ and $U_i^{2\omega}$ is obtained by applying around 2ω (from 1.5ω to 2.5ω) a bandpass filter to each original temporal signal, respectively, in using the system parameters fixed as above: $\gamma = 0.0162$, $\eta = 0.0088$ (corresponding to a Q factor equal to 80), $B_1 = 0.002$ and $B_2 = 0$.

V. CONCLUSION

In conclusion, through designing a nonlinear metasurface with a dual-resonance mass-spring system, we have proven both theoretically and numerically the possibility of achieving a near perfect absorption of the incoming fundamental wave together with its efficient conversion into the second harmonic frequency. If the metasurface lies between a relatively soft propagation medium (air for instance) and a rigid wall and moreover if the metasurface exhibits weak intrinsic dissipation ($Q = 80$), our results indicate that even with a small quadratic nonlinearity ($B_1 = 0.002$), a reflection amplitude at the fundamental incoming wave frequency of $|\tilde{R}(\Omega)| \approx 0.05$ is obtained and a reflected second harmonic of amplitude $|\tilde{R}(2\Omega)| \approx 0.46$ can be reached. In order to study the characteristic frequency bandwidth character of this effect, the nonlinear reflection of a wave packet has also been examined via the numerical integration of the metasurface system of nonlinear motion equations. When the characteristic temporal width of the wave packet signal is large in comparison to the lifetimes of the metasurface two resonances ($\omega T \gg \tau_i$ with $i = 1$, 2), a good level of agreement between the theoretical results obtained by HBM and the implemented numerical results is found, in accordance with expectations. For smaller width however, deviations from the HBM results are observed, indicating that they tend toward the linear reflection results. This funding is explained by the fact that the excitation time is shorter than the time necessary to accumulate nonlinear effects, i.e., the characteristic time τ^{NL}.

The potentially very wide metasurface design space is limited here to the configuration of a dual-resonance system, chosen such that its first resonance frequency equals to the excitation frequency and half the second resonance frequency. Consequently, a number of interesting configurations still need to be studied with detuning, for example, between the interface resonances or between the excitation frequency and the first resonance frequency. Also, as recently demonstrated in Ref. 40, it is possible to design architected materials in order to achieve the desired type (quadratic, cubic) and amount of elastic wave nonlinearity, in addition to designing the linear dispersive properties. This approach opens up avenues for enhancing the possible wave phenomena induced during the reflection process by a nonlinear metasurface, including but not limited to the wave manipulation of intense sounds, energy mitigation, and the linearization of intense sound resonators.

ACKNOWLEDGMENTS

We acknowledge the support of the project "Le Mans Acoustics HUB".

APPENDIX: HARMONIC BALANCE METHOD

According to the harmonic balance method (HBM), the solution U_i ($i = 1$, 2) of the considered problem Eq. (4) can be written in the form of a vector product $U_i(\tau) = \{\mathbf{C}\}^{\mathbf{T}}\{\mathbf{q}\}_i$ with $\{\mathbf{C}\}^{\mathbf{T}}$ the transpose of column vector $\{\mathbf{C}\}$ containing all the sinusoidal terms

$$\{\mathbf{C}\} = \begin{Bmatrix} 1 \\ \cos(\tau) \\ \sin(\tau) \\ \cos(2\tau) \\ \sin(2\tau) \\ \vdots \\ \cos(N\tau) \\ \sin(N\tau) \end{Bmatrix}_{(2N+1)\times 1}, \tag{A1}$$

and $\{\mathbf{q_i}\}$ ($i = 1$, 2) another vector containing all the magnitude terms

$$\{\mathbf{q_i}\} = \{U_{i0}, C_{i1}, S_{i1}, C_{i1}, S_{i1}, \ldots, C_{iN}, S_{iN}\}^{\mathbf{T}}_{(2N+1)\times 1}.$$

The derivatives of displacement $U_i(\tau)$ with respect to τ are $\frac{\partial U_i}{\partial \tau} = \left\{\frac{\partial \mathbf{C}}{\partial \tau}\right\}^{\mathbf{T}}\{\mathbf{q}\}_i$ and $\frac{\partial^2 U_i}{\partial \tau^2} = \left\{\frac{\partial^2 \mathbf{C}}{\partial \tau^2}\right\}^{\mathbf{T}}\{\mathbf{q}\}_i$.

We define the sinusoidal matrix as

$$[\mathbf{S}] = \begin{bmatrix} \{\mathbf{C}\}^T & 0 \\ 0 & \{\mathbf{C}\}^T \end{bmatrix}_{2\times(4N+2)}, \tag{A2}$$

and the magnitude vector as

$$\{\mathbf{q}\} = \begin{Bmatrix} \{\mathbf{q}_1\} \\ \{\mathbf{q}_2\} \end{Bmatrix}_{(4N+2)\times 1}. \tag{A3}$$

Thus, the considered system of motion equation (4) can be re-written in the following matrix form:

$$\Omega^2[\mathbf{M}]\left[\frac{\partial^2 \mathbf{S}}{\partial \tau^2}\right]\{\mathbf{q}\} + \Omega[\mathbf{\Gamma}]\left[\frac{\partial \mathbf{S}}{\partial \tau}\right]\{\mathbf{q}\} + [\mathbf{K}][\mathbf{S}]\{\mathbf{q}\} + [\mathbf{S}]\{\mathbf{U_{inc}}\} = \{\mathbf{F_{NL}}\}, \tag{A4}$$

with the source vector $\{\mathbf{U_{inc}}\}$ written as $\{\mathbf{U_{inc}}\} = \{0, 2, 0, 0, \ldots, 0\}^{\mathbf{T}}_{(4N+2)\times 1}$. The mass matrix $[\mathbf{M}]$, spring matrix $[\mathbf{K}]$, and the damping matrix $[\mathbf{\Gamma}]$ are, respectively,

$$[\mathbf{M}] = \begin{bmatrix} 0.5 & 0 \\ 0 & 1 \end{bmatrix}, \quad [\mathbf{K}] = \begin{bmatrix} 1 & -1 \\ -1 & 3 \end{bmatrix}, \tag{A5}$$

and

$$[\mathbf{\Gamma}] = \begin{bmatrix} (\gamma + \eta_1) & -\eta_1 \\ -\eta_1 & (\eta_1 + \eta_2) \end{bmatrix}. \tag{A6}$$

The nonlinear force $\{\mathbf{F_{NL}}\}$ takes the form

$$\{\mathbf{F_{NL}}\} = \begin{Bmatrix} -f_{NL}^{(1)} \\ f_{NL}^{(1)} - f_{NL}^{(2)} \end{Bmatrix}_{(2\times 1)}, \tag{A7}$$

with $f_{NL}^{(1)} = B_1\{\mathbf{q}\}^{\mathbf{T}}[\mathbf{S}]^{\mathbf{T}}\begin{bmatrix} 1 & -1 \\ -1 & 1 \end{bmatrix}[\mathbf{S}]\{\mathbf{q}\}$ and $f_{NL}^{(2)} = 2B_2\{\mathbf{q}\}^{\mathbf{T}}[\mathbf{S}]^{\mathbf{T}}\begin{bmatrix} 0 & 0 \\ 0 & 1 \end{bmatrix}[\mathbf{S}]\{\mathbf{q}\}$.

Thereafter, the studied matrix-form motion equation system Eq. (A4) can be projected onto the base $[\mathbf{S}]$ as

$$\frac{\Omega^2}{\pi}\int_0^{2\pi}[\mathbf{S}]^T[\mathbf{M}]\left[\frac{\partial^2\mathbf{S}}{\partial\boldsymbol{\tau}^2}\right]\{\mathbf{q}\}d\tau+\frac{\Omega}{\pi}\int_0^{2\pi}[\mathbf{S}]^T[\boldsymbol{\Gamma}]\left[\frac{\partial\mathbf{S}}{\partial\boldsymbol{\tau}}\right]\{\mathbf{q}\}d\tau$$
$$+\frac{1}{\pi}\int_0^{2\pi}[\mathbf{S}]^T[\mathbf{K}][\mathbf{S}]\{\mathbf{q}\}d\tau+\frac{1}{\pi}\int_0^{2\pi}[\mathbf{S}]^T[\mathbf{S}]\{\mathbf{U_{inc}}\}d\tau$$
$$=\frac{1}{\pi}\int_0^{2\pi}[\mathbf{S}]^T\{\mathbf{F_{NL}}\}d\tau, \tag{A8}$$

that is,

$$\Omega^2\left\langle[\mathbf{S}]^T[\mathbf{M}]\left[\frac{\partial^2\mathbf{S}}{\partial\boldsymbol{\tau}^2}\right]\right\rangle\{\mathbf{q}\}+\Omega\left\langle[\mathbf{S}]^T[\boldsymbol{\Gamma}]\left[\frac{\partial\mathbf{S}}{\partial\boldsymbol{\tau}}\right]\right\rangle\{\mathbf{q}\}$$
$$+\langle[\mathbf{S}]^T[\mathbf{K}][\mathbf{S}]\rangle\{\mathbf{q}\}+\langle[\mathbf{S}]^T[\mathbf{S}]\{\mathbf{U}_{inc}\}\rangle=\langle[\mathbf{S}]^T\mathbf{F_{NL}}\rangle, \tag{A9}$$

where $\langle\cdots\rangle$ denotes the integral operator $\frac{1}{\pi}\int_0^{2\pi}(\cdots)d\tau$.

Thanks to this projection, the calculation is simplified because for all positive integers n et m, we have $\frac{1}{\pi}\int_0^{2\pi}\cos(m\tau)\sin(n\tau)d\tau=0$ and

$$\frac{1}{\pi}\int_0^{2\pi}\cos(m\tau)\cos(n\tau)d\tau$$
$$=\frac{1}{\pi}\int_0^{2\pi}\sin(m\tau)\sin(n\tau)d\tau=\begin{cases}0, & if\ m\neq n\neq 0\\ 1, & if\ m=n\neq 0\\ 2, & if\ m=n=0\end{cases}. \tag{A10}$$

In the matrix form motion equation system Eq. (A9), with these integral results, all the linear terms can be simplified and determined analytically. The nonlinear term $\langle[\mathbf{S}]^T\mathbf{F_{NL}}\rangle$ has the following explicit form:

$$\langle[\mathbf{S}]^T\mathbf{F_{NL}}\rangle=B_1\frac{1}{\pi}\int_0^{2\pi}\begin{bmatrix}-[\mathbf{A}] & [\mathbf{A}]\\ [\mathbf{A}] & -[\mathbf{A}]\end{bmatrix}\{\mathbf{q}\}d\tau$$
$$+2B_2\frac{1}{\pi}\int_0^{2\pi}\begin{bmatrix}0 & 0\\ 0 & -[\mathbf{B}]\end{bmatrix}\{\mathbf{q}\}d\tau, \tag{A11}$$

with $[\mathbf{A}]=\{\mathbf{C}\}\{\Delta q\}^{\mathbf{T}}\{\mathbf{C}\}\{\mathbf{C}\}^{\mathbf{T}}$, $[\mathbf{B}]=\{\mathbf{C}\}\{\mathbf{q}_2\}^{\mathbf{T}}\{\mathbf{C}\}\{\mathbf{C}\}^{\mathbf{T}}$, and with $\{\Delta q\}^{\mathbf{T}}=\{\mathbf{q}_1\}^{\mathbf{T}}-\{\mathbf{q}_2\}^{\mathbf{T}}$.

The integrals $\frac{1}{\pi}\int_0^{2\pi}[\mathbf{A}]d\tau$ and $\frac{1}{\pi}\int_0^{2\pi}[\mathbf{B}]d\tau$ can respectively be written as

$$\left[\frac{1}{\pi}\int_0^{2\pi}[\mathbf{A}]d\tau\right]_{ij}=\sum_m\Delta q_m\frac{1}{\pi}\int_0^{2\pi}C_iC_mC_jd\tau, \tag{A12}$$

and

$$\left[\frac{1}{\pi}\int_0^{2\pi}[\mathbf{B}]d\tau\right]_{ij}=\sum_m q_{2m}\frac{1}{\pi}\int_0^{2\pi}C_iC_mC_jd\tau, \tag{A13}$$

containing integrals that can be numerically evaluated.

With all the explicit forms of the terms of Eq. (A9), the considered problem can be solved numerically by the Newton-Raphson method.

The main steps of the numerical calculation are recalled here:

1. Write the considering Eq. (A9) in the matrix form of $\mathbf{F}(\mathbf{q})=0$ (with N harmonics), calculate the linear solution $\{\mathbf{q_L}\}$ (with $B_i=0$) of the system, and input it as the initial value of $\{\mathbf{q}_1\}=\{\mathbf{q_L}\}$.
2. For the next iteration $n+1$, according to the Newton-Raphson method, we have

$$\mathbf{q}_{n+1}=\mathbf{q}_n-\left[\mathbf{J}(\mathbf{q}_n)\right]^{-1}\mathbf{F}(\mathbf{q}_n), \tag{A14}$$

with $[\mathbf{J}(\mathbf{q}_n)]^{-1}$ the inverse of Jacobian matrix $[\mathbf{J}(\mathbf{q}_n)]$ which can be obtained by

$$[\mathbf{J}(\mathbf{q_n})]_{ij}=\frac{\partial\mathbf{F}(\mathbf{q_n})_i}{\partial(\mathbf{q_n})_j}. \tag{A15}$$

For the considered problem

$$\mathbf{F}(\mathbf{q})=\Omega^2\left\langle[\mathbf{S}]^{\mathbf{T}}[\mathbf{M}]\left[\frac{\partial^2\mathbf{S}}{\partial\boldsymbol{\tau}^2}\right]\right\rangle\{\mathbf{q}\}+\langle[\mathbf{S}]^{\mathbf{T}}\mathbf{F_L}\rangle-\langle[\mathbf{S}]^{\mathbf{T}}\mathbf{F_{NL}}\rangle=0, \tag{A16}$$

with

$$\langle[\mathbf{S}]^{\mathbf{T}}\mathbf{F_L}\rangle=\langle[\mathbf{S}]^{\mathbf{T}}[\mathbf{K}][\mathbf{S}]\rangle\{\mathbf{q}\}+\Omega\left\langle[\mathbf{S}]^{\mathbf{T}}[\boldsymbol{\Gamma}]\left[\frac{\partial\mathbf{S}}{\partial\boldsymbol{\tau}}\right]\right\rangle\{\mathbf{q}\}$$
$$+\langle[\mathbf{S}]^{\mathbf{T}}[\mathbf{S}]\{\mathbf{U}_{inc}\}\rangle. \tag{A17}$$

The Jacobian matrix takes the form

$$[\mathbf{J}(\mathbf{q_n})]_{ij}=\Omega^2\left\langle[\mathbf{S}]^{\mathbf{T}}[\mathbf{M}]\left[\frac{\partial^2\mathbf{S}}{\partial\boldsymbol{\tau}^2}\right]\right\rangle_{ij}+\langle[\mathbf{S}]^{\mathbf{T}}[\mathbf{K}][\mathbf{S}]\rangle_{ij}$$
$$+\Omega\left\langle[\mathbf{S}]^{\mathbf{T}}[\boldsymbol{\Gamma}]\left[\frac{\partial\mathbf{S}}{\partial\boldsymbol{\tau}}\right]\right\rangle_{ij}-\frac{\partial\langle[\mathbf{S}]^{\mathbf{T}}\mathbf{F_{NL}}\rangle_i}{\partial(\mathbf{q_n})_j}. \tag{A18}$$

Notice that all the linear terms can be directly determined, and only the nonlinear part $\frac{\partial\langle[\mathbf{S}]^{\mathbf{T}}\mathbf{F_{NL}}\rangle_i}{\partial(\mathbf{q_n})_j}$ should be numerically calculated. By using the Einstein notation, we find finally that

$$\frac{\partial\langle[\mathbf{S}]^{\mathbf{T}}\mathbf{F_{NL}}\rangle_i}{\partial(\mathbf{q_n})_j}=\begin{bmatrix}-[\mathbf{P}] & +[\mathbf{P}]\\ +[\mathbf{P}] & -[\mathbf{P}]-[\mathbf{Q}]\end{bmatrix}, \tag{A19}$$

with

$$[\mathbf{P}]_{ij}=2B_1\sum_m\frac{1}{\pi}\int_0^{2\pi}(C_i\,\Delta q_m^{\mathbf{T}}C_mC_j^{\mathbf{T}})d\tau, \tag{A20}$$

and

$$[\mathbf{Q}]_{ij}=4B_2\sum_m\frac{1}{\pi}\int_0^{2\pi}(C_i\,q_{2m}^{\mathbf{T}}C_mC_j^{\mathbf{T}})d\tau, \tag{A21}$$

where $\Delta q_m^{\mathbf{T}}=q_{1m}^{\mathbf{T}}-q_{2m}^{\mathbf{T}}$ $(m=1,2,\ldots,2N+1)$.

3. For each iteration $n+1>1$, we define the relative error as

$$\epsilon_n=\sqrt{\frac{\Sigma_{i=1}^{4N+2}|\{\mathbf{q}_{n+1}\}_i-\{\mathbf{q}_n\}_i|^2}{\Sigma_{i=1}^{4N+2}|\{\mathbf{q}_{n+1}\}_i|^2}}. \tag{A22}$$

An acceptable value of this relative error is put at $\epsilon_c=10^{-6}$ in the present study. The loop goes on until the relative error is smaller than this given value.

4. When $\epsilon_n \leq \epsilon_c$, the loop is stopped and the solution U_i of the considered problem is obtained. Therefore, the reflection coefficients $\tilde{R}_n$ $(1 \leq n \leq N)$ for all the signal harmonics are determined: $\tilde{R}_n = \delta_n^1 + in\gamma\Omega(C_{in} - iS_{in})$.

[1]P. A. Deymier, *Acoustic Metamaterials and Phononic Crystals* (Springer, 2013).
[2]R. V. Craster and S. Guenneau, *Acoustic Metamaterials-Negative Refraction, Imaging, Lensing and Cloaking*, Springer Series in Materials Science (Springer, Netherlands, 2012).
[3]T. J. Cui, D. Smith, and R. Liu, *Metamaterials - Theory, Design, and Applications* (Springer, 2010).
[4]M. Oudich, Y. Li, B. M. Assouar, and Z. Hou, New J. Phys. **12**, 083049 (2010).
[5]C. Lagarrigue, J. P. Groby, and V. Tournat, J. Acoust. Soc. Am. **133**, 247 (2013).
[6]G. Ma, M. Yang, S. Xiao, Z. Yang, and P. Sheng, Nat. Mater. **13**, 873 (2014).
[7]A. Santillán and S. I. Bozhevolnyi, Phys. Rev. B **84**, 064304 (2011).
[8]G. Theocharis, O. Richoux, V. Romero-Garcia, A. Merkel, and V. Tournat, New J. Phys. **16**, 093017 (2014).
[9]A. Santillán and S. I. Bozhevolnyi, Phys. Rev. B **89**, 184301 (2014).
[10]V. M. Agranovich, Y. R. Shen, R. H. Baughman, and A. A. Zakhidov, Phys. Rev. B **69**, 165112 (2004).
[11]G. V. Eleftheriades and K. G. Balmain, *Negative-Refraction Metamaterials: Fundamental Principles and Applications* (Wiley/IEEE Press, 2005).
[12]J. Yao, Z. Liu, Y. Liu, Y. Wang, C. Sun, G. Bartal, A. M. Stacy, and X. Zhang, Science **321**, 930 (2008).
[13]J. Li and C. T. Chan, Phys. Rev. E **70**, 055602 (2004).
[14]D. R. Smith, J. B. Pendry, and M. C. K. Wiltshire, Science **305**, 788 (2004).
[15]J. Christensen, Z. Liang, and M. Willatzen, Phys. Rev. B **88**, 100301 (2013).
[16]T. Devaux, V. Tournat, O. Richoux, and V. Pagneux, Phys. Rev. Lett. **115**, 234301 (2015).
[17]F. Lemoult, N. Kaina, M. Fink, and G. Lerosey, Crystals **6**, 82 (2016).
[18]Y. Li, S. Qi, and B. M. Assouar, New J. Phys. **18**, 043024 (2016).
[19]C. Lagarrigue, J. P. Groby, V. Tournat, O. Dazel, and O. Umnova, J. Acoust. Soc. Am. **134**, 4670 (2013).
[20]V. Romero-García, G. Theocharis, O. Richoux, A. Merkel, V. Tournat, and V. Pagneux, Sci. Rep. **6**, 19519 (2016).
[21]X. Jiang, B. Liang, R. Li, X. Zou, L. Yin, and J. Cheng, Appl. Phys. Lett. **105**, 243505 (2014).
[22]M. Yang, G. Ma, Z. Yang, and P. Sheng, EPJ Appl. Metamater. **2**, 10 (2015).
[23]J. Mei, G. Ma, M. Yang, Z. Yang, W. Wen, and P. Sheng, Nat. Commun. **3**, 756 (2012).
[24]Y. Li and B. M. Assouar, Appl. Phys. Lett. **108**, 063502 (2016).
[25]M. Yang, C. Meng, C. Fu, Y. Li, Z. Yang, and P. Sheng, Appl. Phys. Lett. **107**, 104104 (2015).
[26]Y. Duan, J. Luo, G. Wang, Z. H. Hang, B. Hou, J. Li, P. Sheng, and Y. Lai, Sci. Rep. **5**, 12139 (2015).
[27]P. Sheng, J. Acoust. Soc. Am. **141**, 3575 (2017).
[28]W. Cai, U. K. Chettiar, A. V. Kildishev, and V. M. Shalaev, Nat. Photonics **1**, 224 (2007).
[29]J. Valentine, J. Li, T. Zentgraf, G. Bartal, and X. Zhang, Nat. Mater. **8**, 568 (2009).
[30]G. Zhu, J. Appl. Phys. **113**, 163103 (2013).
[31]B.-I. Popa, L. Zigoneanu, and S. A. Cummer, Phys. Rev. B **88**, 024303 (2013).
[32]O. R. Bilal, A. Foehr, and C. Daraio, Proc. Natl. Acad. Sci. U.S.A. **114**, 4603 (2017).
[33]O. R. Bilal, A. Foehr, and C. Daraio, Adv. Mater. **29**, 1700628 (2017).
[34]N. Boechler, G. Theocharis, and C. Daraio, Nat. Mater. **10**, 665 (2011).
[35]R.-Q. Li, B. Liang, Y. Li, W.-W. Kan, X.-Y. Zou, and J.-C. Cheng, Appl. Phys. Lett. **101**, 263502 (2012).
[36]J.-S. Chen, I.-L. Chang, W.-T. Huang, L.-W. Chen, and G.-H. Huang, AIP Adv. **6**, 095020 (2016).
[37]J. Christensen and F. J. G. de Abajo, Phys. Rev. Lett. **108**, 124301 (2012).
[38]J. Cabaret, P. Béquin, G. Theocharis, V. Andreev, V. E. Gusev, and V. Tournat, Phys. Rev. Lett. **115**, 054301 (2015).
[39]C. Daraio, V. F. Nesterenko, E. B. Herbold, and S. Jin, Phys. Rev. E **73**, 026610 (2006).
[40]B. Deng, J. R. Raney, V. Tournat, and K. Bertoldi, Phys. Rev. Lett. **118**, 204102 (2017).
[41]V. Grubsky and A. Savchenko, Opt. Express **13**, 6798 (2005).
[42]S. Sun, N. Yi, W. Yao, Q. Song, and S. Xiao, Opt. Express **22**, 26613 (2014).
[43]L. Wang, J.-H. Zhang, Z.-Q. Wang, C. Liu, M. Li, F.-H. Qi, and R. Guo, Phys. Rev. E **93**, 012214 (2016).
[44]R. A. Van Gorder, Phys. Rev. D **95**, 096007 (2017).
[45]C. G. Biris and N. C. Panoiu, Phys. Rev. B **81**, 195102 (2010).
[46]M. Hamilton and D. Blackstock, *Nonlinear Acoustics* (Elsevier Science Publishing Co. Inc., 1997).
[47]S. Shan, S. H. Kang, J. R. Raney, P. Wang, L. Fang, F. Candido, J. A. Lewis, and K. Bertoldi, Adv. Mater. **27**, 4296 (2015).
[48]B. Florijn, C. Coulais, and M. van Hecke, Phys. Rev. Lett. **113**, 175503 (2014).
[49]K. Bertoldi and M. C. Boyce, Phys. Rev. B **77**, 052105 (2008).
[50]P. Wang, F. Casadei, S. Shan, J. C. Weaver, and K. Bertoldi, Phys. Rev. Lett. **113**, 014301 (2014).
[51]J. Cabaret, V. Tournat, and P. Béquin, Phys. Rev. E **86**, 041305 (2012).
[52]V. Marinca and N. Herisanu, "The method of harmonic balance," in *Nonlinear Dynamical Systems in Engineering: Some Approximate Approaches* (Springer, Berlin, Heidelberg, 2011), pp. 31–45.
[53]E. Hairer, S. P. Nørsett, and G. Wanner, "Runge-kutta and extrapolation methods," in *Solving Ordinary Differential Equations I: Nonstiff Problems* (Springer, Berlin, Heidelberg, 1993), pp. 129–353.